Yeliz Pekbey*, Goudarz Ghanizadeh Hesar, Hasan Yildiz and Farshid Khosravi Maleki

Determination of the critical load and energy release rate in mode II delamination using a meshfree method

Abstract: Simulation of fracture by using numerical methods is important to treat geometries that change in time. In this study, both numerical and experimental investigations are presented for the delamination under mode II loading, detailing the derivation of the formulations in numerical simulations of fracture. The simulation of the delamination under mode II loading based on the cohesive segments model was investigated by using a meshfree method. Then, an experimental investigation was used to verify the meshfree method's results. For tests under mode II loading, three-point end-notched flexure specimens, which are made of carbon/epoxy laminate (AS4/3501-6) which consists of 10 plies in $[0]_{10}$ and $[0/90/0/90/0]_s$ lay-up with delamination inserted in the middle of the laminate, were used for the interlaminar fracture toughness tests. The problem was solved for $[0]_{10}$, $[0/45/-45/90/0]_s$, $[0/90/0/90/0]_s$, $[0/90/0/90/30]_s$, $[0/90/0/90/45]_s$ and $[0/90/0/90/60]_s$ laminates with midplane delaminations, and the results were verified for different composite materials. The critical fracture force, which can be experimentally measured, was used to calculate the mode II delamination fracture toughness of the carbon/epoxy laminate. In addition, values of the integral for 209 (11×19) and 253 (11×23) background meshes with equivalent interval sizes were compared. For a relatively fine background mesh, the critical load was converged. Results obtained from the meshfree element-free Galerkin method showed very good agreement with experimental data for single-mode delamination under mode II loading. The results presented will help in the implementation of mesh design techniques that protect numerical accuracy while minimizing computational expense.

Keywords: delamination fracture toughness; energy release rate; mode II loading.

***Corresponding author: Yeliz Pekbey,** Ege University Department of Mechanical Engineering, Izmir, Turkey,
e-mail: pekbey.yeliz@gmail.com
Goudarz Ghanizadeh Hesar, Hasan Yildiz and Farshid Khosravi Maleki: Ege University Department of Mechanical Engineering, Izmir, Turkey

1 Introduction

Delamination is one of the most common types of damage in composites because of their relatively weak interlaminar strengths. Delamination may appear under various conditions such as transverse concentrated loads. This damage mode is especially important for the structural integrity of composite structures since it is difficult to detect during inspection. It has a detrimental influence on both stiffness and strength of structural components. In order to use the full capacity of a composite structure, it is important that the initiation of delamination cracks and the resulting reduction in laminate strength can be correctly modeled. Therefore, a significant research effort has been devoted to studying the laws governing the onset and evolution of delamination damage [6]. It is interesting to predict whether the delamination will grow as the structure is loaded.

Delamination of laminated composite structures has been widely examined, from both an experimental and a numerical standpoint, due to local failure and, sometimes, to sudden structural collapse. Therefore, knowledge of delamination modes and growth rate during the operating life of a composite structure is of primary concern. Several studies aimed at formulating a criterion for delamination onset and growth prediction have been published, and experimental testing was performed for validating theoretical models. An opening mode (mode I) and a shearing mode (mode II) are the main modes of fracture in composites. There are existing standard tests for determining the critical strain energy release rates associated with each mode. The criteria used to predict delamination propagation under mode loading conditions are usually established in terms of the components of the energy release rate (G_I, G_{II}, G_{III}) and fracture toughness (G_{IC}, G_{IIC}, G_{IIIC}). The strain energy release rate (G) is often appraised because of an experimentally measurable quantity and it has been mathematically well defined. Delamination propagation is predicted when the energy release rate is equal to the corresponding fracture toughness of the material. Therefore, several fracture test methods have been developed

to measure the critical strain energy release rates for pure and mixed-mode loadings.

Numerical simulation of the delamination is based on either fracture mechanics or damage mechanics. Linear elastic fracture mechanics (LEFM) is used if the material nonlinearities can be neglected. Delamination growth of one or more cracks is predicted using LEFM. The assumption is that the delamination propagates when the associated energy release rate is greater than or equal to a critical value. The application of this method is easy since the crack front propagates in one dimension. When more than one crack propagates simultaneously, the mechanical behavior of the interface which includes the cohesive zone model is modeled on the basis of damage mechanics. The interface-traction relationship is based on a simple bilinear one-dimensional law. The area of the triangle delimited by the traction/relative displacement curve is equated to the critical energy release rate [1].

Computational methods such as the finite differences method (FDM), the finite element method (FEM) or the finite volume method (FVM) all make use of a mesh, i.e., a set of nodes with node-to-node connectivity, which has gained much attention over the last 10 years. Since these methods have been successfully used to solve engineering problems for decades, some limitations of these kinds of methods are becoming more and more obvious: mesh generation is very time consuming and, in problems with moving boundaries, a drastic loss of accuracy is observed due to the distortion of the elements. Therefore there is a need to develop meshfree (grid free, mesh less) methods that do not suffer from the problems described above. Meshfree methods and application of composite fracture continue to be used in in-depth research. Meshfree methods are very widely used for modeling problems with moving boundaries such as crack growth in solids, because changing discontinuities can be displayed very easily by modifying only the weighting functions, which is a well-known advantage compared to the classical finite element method. In the meshfree method, discontinuities are not restricted to element boundaries or even no elements are necessary at all. Only nodes are used for approximation [3, 9, 14].

Meshfree methods have existed for a number of years, and the element-free Galerkin (EFGM) was first proposed for the simulation of fracture 15 years ago by Belytschko et al. [4, 5]. Several review articles [2, 7, 8, 10, 11], which cover the classification, application and computer implementation aspects of the meshfree method, have been reported in the literature [12–22].

The aim of this study was to present a meshfree method for the simulation of the delamination and failure of composite materials based on the cohesive segments model. With the use of the partition of unity of moving least-squares (MLS) shape functions, the discontinuities at the cohesive segments can be approximated with the additional degrees of freedom of nodes. An iterative solution scheme between the continuous and discontinuous fields is presented to solve the mode II delamination growth problem. An experimental investigation was used to verify the meshfree method's results. The experimental study used end-notched flexure (ENF) specimens made of carbon/epoxy laminate (AS4/3501-6) which consists of 10 plies in $[0]_{10}$ and $[0/90/0/90/0]_s$ lay-up with delamination inserted in the middle of the laminate.

The problem was solved for $[0]_{10}$, $[0/45/-45/90/0]_s$, $[0/90/0/90/0]_s$, $[0/90/0/90/30]_s$, $[0/90/0/90/45]_s$ and $[0/90/0/90/60]_s$ laminates with mid-plane delaminations, and the results are verified for different composite materials. The critical fracture force, which can be experimentally measured, was used to calculate the mode II delamination fracture toughness for the carbon/epoxy laminate. In addition, values of the integral for 219 (11×19) and 253 (11×23) background meshes with equivalent interval sizes were compared.

2 The meshfree method

A number of different meshfree methods have been developed. One of the most widely used is the EFGM. This method implements the connectivity between the nodes and sets completely using approximation functions. The EFGM uses the moving least-squares (MLS) approximants in order to obtain test and trial functions; background cells are utilized for numerical integration in the weak form; and essential boundary conditions are implemented using Lagrange multipliers. The weak form of Galerkin was used to develop the discretized system of equations.

The meshfree method is described in a broad sense as a method where nodes are not required to be interconnected. A distribution of nodes is generated to define the domain and its boundaries, and the solution of the problem is sought at these nodes in the EFGM. However, cells are also prescribed over the domain and used for numerical integration. In the EFGM, the moving least squares (MLS) scheme is utilized for interpolation, and a mesh of background cells, with no required connection to the nodal discretization, is used for the purpose of numerical integration [11].

2.1 The moving least-squares shape functions

In this section, we will explain the moving least square (MLS) method and establish the connections between the weighting coefficients and the partial derivatives of the MLS shape functions. The approximation $u(x)$ of the function $u(x)$ is defined in the domain Ω as

$$u^h(x)=\sum_{j=1}^{m} P_j(x)a_j(x)=P^{\mathrm{T}}(x)a(x) \tag{1}$$

where $P_j(x)$, $j=1,2...,m$ are monomial basis functions and $a_j(x)$ are unknown coefficients. The unknown coefficient $a_j(x)$ can be achieved such that the weighted difference between the approximate values at nodes nearby and the nodal values is minimized. These coefficients are obtained, at any point x, minimizing the weighted discrete norm J,

$$J=\sum_{i=1}^{n} \hat{W}(x-x_i)[P^{\mathrm{T}}(x_i)a(x)-u_i]^2 \tag{2}$$

where n and u_i are the number of nodes in the domain of influence of x and the nodal parameter of $u(x)$ at $x=x_i$, respectively. Because of the limited number of nodes close to the evaluation point, the MLS approximation is local. The size of the domain influence identifies the number of discrete points in the domain of influence. The kernel $\hat{W}(x-x_i)$ or weight function, which is positive, decreases as $||x-x_i||$ increases. $||x-x_i||$ is defined as the distance between the node x_i and the sampling point x in the domain of influence. The choice of the weight function is important due to the effect on the performance of the EFGM [5]. The cubic spline weight function [Eq. (3)], quadratic spline function [Eq. (4)] and exponential function [Eq. (5)] are generally used as weight functions in the one-dimensional case.

$$\hat{W}_i(x)=\begin{cases} 2/3-4\bar{r}_i^2+4\bar{r}_i^3 & \bar{r}_i\le 0.5 \\ 4/3-4\bar{r}_i+4\bar{r}_i^2-4/3\bar{r}_i^3 & 0.5<\bar{r}_i\le 1 \\ 0 & \bar{r}_i>1 \end{cases} \tag{3}$$

$$\hat{W}_i(x)=\begin{cases} 1-6\bar{r}_i^2+8\bar{r}_i^3-3\bar{r}_i^4 & \bar{r}_i\le 1 \\ 0 & \bar{r}_i>1 \end{cases} \tag{4}$$

$$\hat{W}_i(x)=\begin{cases} e_i^{-(\bar{r}_i/\alpha)^2} & \bar{r}_i\le 1 \\ 0 & \bar{r}_i>1 \end{cases} \tag{5}$$

where α is a constant and r is the normalized distance,

$$\bar{r}_i=\frac{d_i}{d_s}=\frac{\sqrt{(x-x_i)^2+(y-y_i)^2}}{d_s}. \tag{6}$$

The approximate function $u(x)$ can then be expressed in terms of the MLS nodal shape functions as

$$u^h(x)=\sum_{i}^{n}\phi_i(x)u_i \tag{7}$$

$$u^h{}_{(2\times1)}=\begin{Bmatrix} u \\ v \end{Bmatrix}=\begin{bmatrix} \phi_1 & 0 & \dots & \phi_n & 0 \\ 0 & \phi_1 & \dots & 0 & \phi_n \end{bmatrix}\begin{Bmatrix} u_1 \\ v_1 \\ \vdots \\ u_n \\ v_n \end{Bmatrix}=\Phi_{(2\times2n)}u_{(2n\times1)} \tag{8}$$

where $\phi_i(x)$ is the shape function and n is the number of nodes with domains of influence containing the point x. The shape functions constructed with respect to MLS have compact support, or domain of influence, which is identical to the support of the corresponding weight function. The support can be of arbitrary shapes, such as circular, rectangular and square. The two popular types of support are circular and rectangular.

3 Cohesive zone model approach

The cohesive zone model approach is one of the most commonly used tools to investigate interfacial fracture. This approach gives the physical explanations of the failure process and it can be used for both damage tolerance and strength analysis. The cohesive zone model approach is defined by a bilinear constitutive law. In the cohesive zone model, relative displacements and stresses are defined as failure and they do not contain crack tip stress singularities. The fracture process region chosen is a narrow band of vanishing thickness ahead of a crack tip. Bonding of the surfaces of the region is caused by cohesive traction which follows a cohesive constitutive law. There are an initial high positive stiffness and a negative tangent stiffness representing softening. The constitutive law is a bilinear softening model which is regulated by both material strength parameters and fracture mechanics parameters. If the cohesive traction disappears, crack growth takes place. A critical strain energy release rate is equal to the amount of work done per unit area of crack surface.

Consider a domain Ω containing a material discontinuity Γ_c, which divides the domain Ω into two parts: Ω_1 and, under crack, Ω_2. The stress field inside the domain σ

is related to the external loading and to the closing tractions in the material discontinuity through the equilibrium equations. The solid can be loaded by body force b and surface traction (force) t in any distributed fashion in the volume of the solid and the traction $\tau(v)$ in the boundary Γ_c. The traction τ depends on the displacement jump v on the cohesive segment Γ_c.

The bilinear law is the most commonly utilized cohesive law because of its simplicity. The bilinear constitutive relationship is shown in Figure 2 for the softening traction-displacement curves of the interface material model for the cases of mode II delamination. The fracture toughness G_c, cohesive surface tractions τ and the cracking relative displacements v are input material properties. The onset displacement jump and final displacement jump are defined as v_0 and v_f, respectively. The area under the traction-displacement jump relation is defined as the fracture toughness or the critical fracture energy.

The bilinear stress relative displacement curve is composed of three main parts: elastic part, softening part and decohesion part. The constitutive equations are as follows:

$$\tau(v)=[1-D(v)]K_0 v \tag{9}$$

where K_0 is the interface stiffness, D is a damage parameter whose initial value is 0. D starts growing when $v>v_0$ and reaches the value when $v>v_f$. The damage parameter can be computed with the following relations for the elastic part, softening part and decohesion part, respectively:

$$\text{Elastic part: } v\langle v_0,\ D(v)=0 \tag{10}$$

$$\text{Softening part: } v_0\langle v\le v_f, D(v)=\frac{v_f(v-v_0)}{v(v_f-v_0)} \tag{11}$$

$$\text{Decohesion part: } v\rangle v_f,\ D(v)=1 \tag{12}$$

If the traction across the interface increases to the maximum, this part is defined as the elastic part. In the softening part, the traction across the interface decreases to zero. Also, two layers begin to separate from each other in the softening part. If there is no bond between the two layers, the traction across the interface is null. This case is defined as the decohesion part.

Damage initiation is related to the interfacial strength τ_m, i.e., the maximum traction on the traction-displacement jump relation. When v_0 is reached, the stress is equal to the interfacial tensile strength τ_m, the maximum stress level possible. For higher relative displacements, the interface accumulates damage and its ability to sustain stress decreases progressively. Once v exceeds v_f, the interface is fully debonded and it is no longer able to support any stress. If the load were removed after v_0 has been exceeded but before v_f has been reached, the model would unload to the origin. The slope of the constitutive equation before damage initiation K_0 is referred to as the interface stiffness [3, 19, 20].

The criteria used to predict delamination propagation are usually established in terms of the components of the energy release rate and fracture toughness. It is supposed that when the energy release rate G exceeds the critical value, delamination of the critical energy release rate G_C grows.

As illustrated in Figure 1, the shaded area under the τ-v curve is the energy dissipated per unit area; it is defined as the strain energy release rate and the two following relations exist among these parameters:

$$G_c=\int_0^{v_f}\tau\,\mathrm{d}v=\frac{1}{2}v_f\tau_m \tag{13}$$

$$v_0=\frac{\tau_m}{K_0} \tag{14}$$

As shown in Figures 1 and 2, v_3^0 and v_3^f are expressed as the displacement jumps corresponding to delamination onset in mode II and in shear mode, respectively, while N_3^0 and N_3^f are defined as the mode interlaminar strengths. The following relations exist:

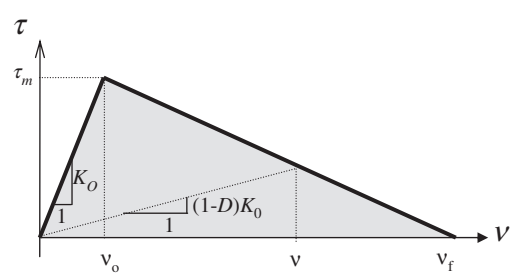

Figure 1 Bilinear interface traction for mode II delamination.

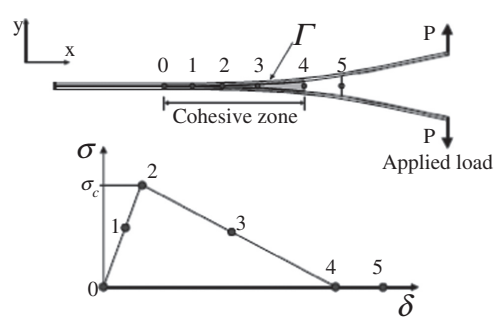

Figure 2 Cohesive zone ahead of delamination tip.

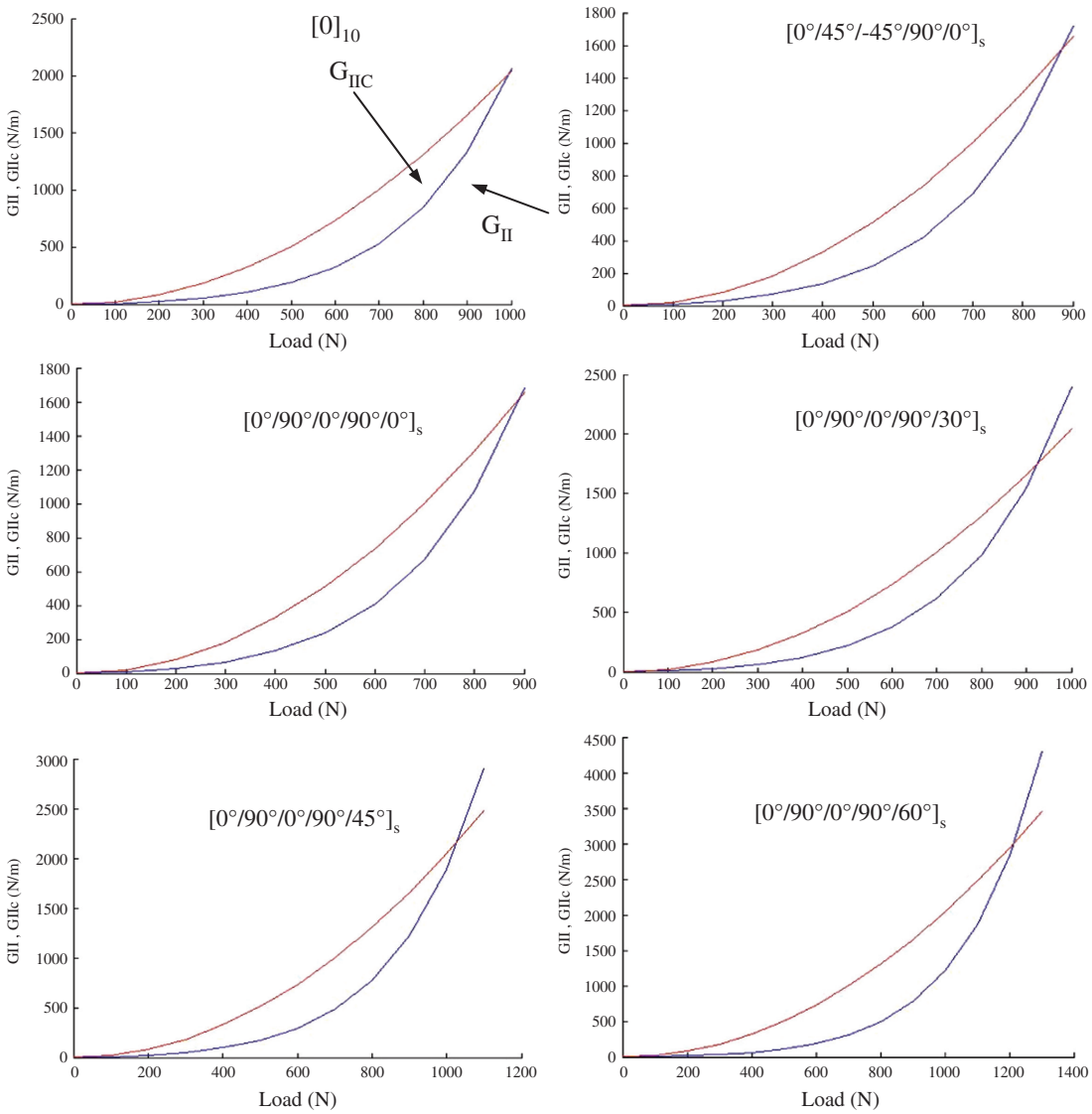

Figure 3 Energy release rate-load diagram for e-glass/epoxy obtained from meshfree method.

$$v_3^0=\frac{N_3^0}{K};v_3^f=\frac{N_3^f}{K}. \tag{15}$$

The opening values v_i are determined by equating the area under the curve to the critical fracture energies such that

$$v_3^f=\frac{2G_{IIC}}{K}. \tag{16}$$

The work done per unit area upon complete interface degradation is given by the integration of cohesive tractions as functions of the displacement jump,

$$G_{IIC}=\int_0^{v_2^f}\tau_{12}\mathrm{d}v_2. \tag{17}$$

where G_{IIC}, τ_{12} and v_3^f are the critical strain energy release rate, the mode traction and the final relative displacements, respectively, corresponding to complete decohesion. A failure criterion for mode II delamination can be written when the following condition is fulfilled:

$$\frac{G_{II}}{G_{IIC}}=1. \tag{18}$$

The existing literature [2] expression utilizes the interface as a resin-rich zone of small thickness e_i and has proposed to define stiffness as:

$$K_x=\frac{E_3}{e},K_y=\frac{G_{13}}{e} \tag{19}$$

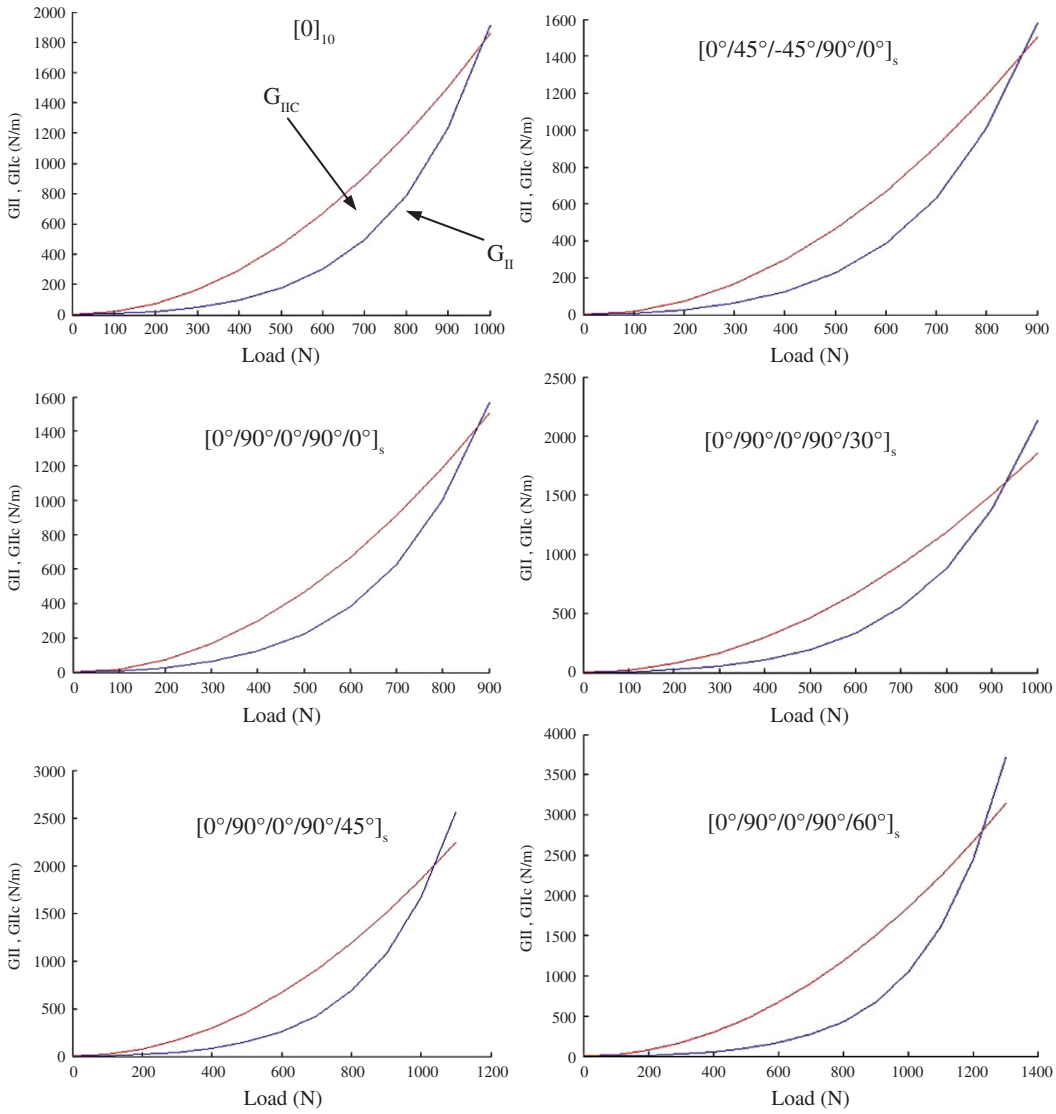

Figure 4 Energy release rate-load diagram for s-glass/epoxy obtained from meshfree method.

where it is assumed that $E_3=E_2$ and $G_{13}=G_{12}$. E_2 and E_3 are Young's modulus in the transverse and thickness direction, respectively.

The stress-relative displacement relationship and the displacement jump can be formulated, respectively, as [3]:

$$\tau=\begin{bmatrix}\tau_x\\ \tau_y\end{bmatrix}=\begin{bmatrix}K_x(v_x,v_y) & 0\\ 0 & K_y(v_x,v_y)\end{bmatrix}\begin{bmatrix}v_x\\ v_y\end{bmatrix}=\begin{bmatrix}(1\text{-}D_x(v_x,v_y))K_{0_x} & 0\\ 0 & (1\text{-}D_y(v_x,v_y))K_{0_y}\end{bmatrix}\begin{bmatrix}v_x\\ v_y\end{bmatrix} \tag{20}$$

$$v=\begin{bmatrix}v_x\\ v_y\end{bmatrix}=\begin{bmatrix}\phi_{1c}{}^{T}U_1 & \phi_{2c}{}^{T}U_2\\ \phi_{1c}{}^{T}V_1 & \phi_{1c}{}^{T}V_2\end{bmatrix}=\begin{bmatrix}\phi_{1c}{}^{T} & 0 & \phi_{2c}{}^{T} & 0\\ 0 & \phi_{1c}{}^{T} & 0 & \phi_{2c}{}^{T}\end{bmatrix} \tag{21}$$

where Φ is the shape function belonging to sub-domain Ω_1 and Ω_2:

$$\phi^{T}=\begin{bmatrix}\phi_{1c}{}^{T} & 0 & \phi_{2c}{}^{T} & 0\\ 0 & \phi_{1c}{}^{T} & 0 & \phi_{2c}{}^{T}\end{bmatrix} \tag{22}$$

4 Variational principle

The EFGM is formulated in the space coordinates $x=[x, y]$ on the domain Ω bounded by Γ. The equilibrium equation can be written at a material point **x** as follows:

$$L^{T}\sigma+b=0 \quad \text{in} \quad \Omega \tag{23}$$

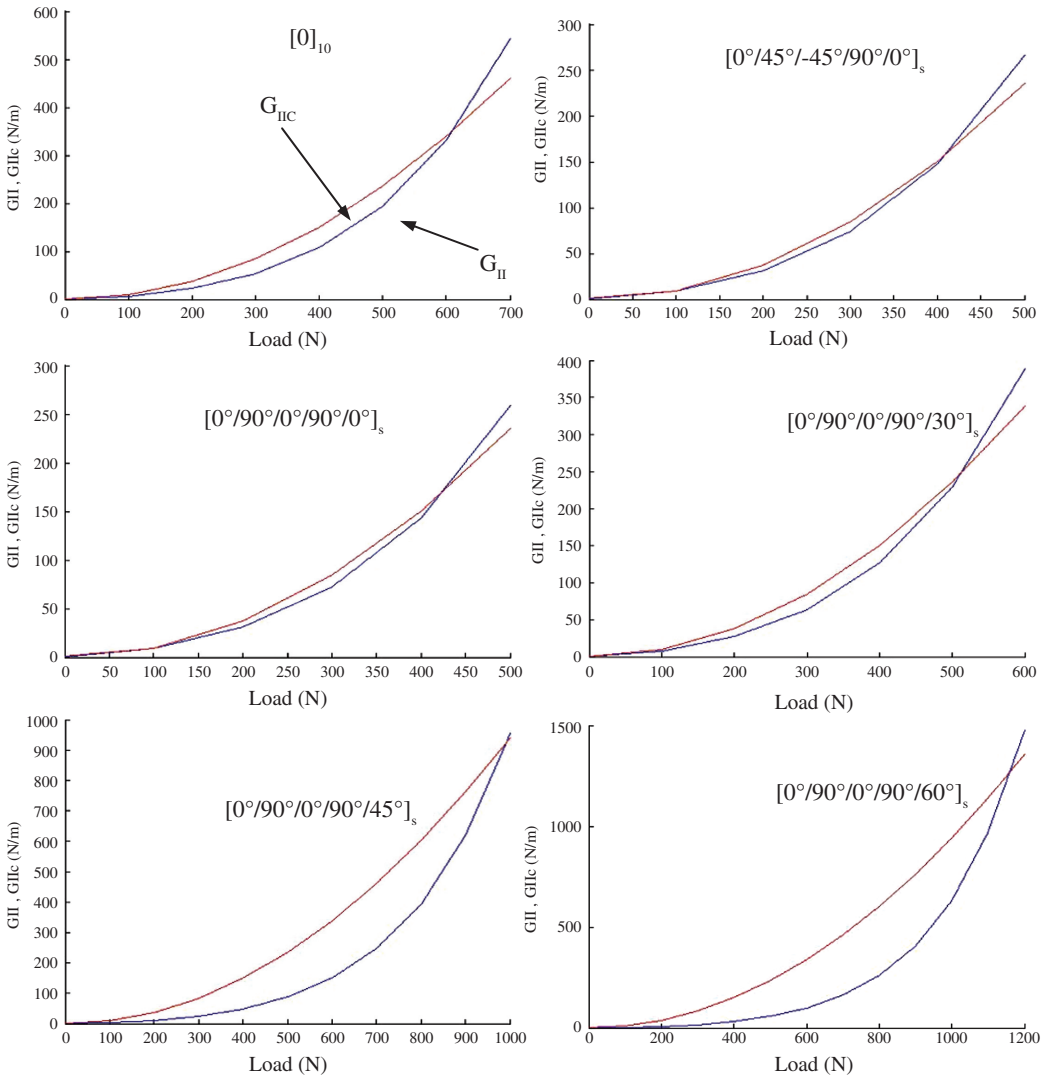

Figure 5 Energy release rate-load diagram for Kevlar/epoxy (Aramid149/epoxy) obtained from meshfree method.

where σ is the stress tensor, which corresponds to the displacement field u, and $\mathbf{b}$ is the body force vector. The boundary conditions are written as $\sigma\cdot\mathbf{n}_c=\tau(v)$ on Γ_c, $\sigma\cdot\mathbf{n}_t=\bar{t}$ on Γ_t and $u=\bar{u}$ on Γ_u, where $\bar{t}$ and $\bar{u}$ are defined as traction on the traction (natural) boundaries and as displacement on the displacement (essential) boundaries; $\mathbf{n}_t$ is the normal unity vector of the boundary Γ_t where the traction $\bar{t}$ is prescribed; $\mathbf{n}_c$ is the normal unity vector of the boundary Γ_c where the traction $\tau(v)$ is prescribed; and Γ_u is the boundary where the displacement $\bar{u}$ is imposed.

The boundary conditions in the EFGM cannot be performed as in classical computational techniques because the properties of Kronecker delta are not satisfied. Therefore special methods are required such as the Lagrange multipliers method, coupling with FEM, and penalty methods. In this study, Lagrange multipliers were used. The weak form is written with Lagrange multipliers, with essential boundary conditions [3]:

$$\int_{\Omega_1}\delta(Lu)^{\mathrm{T}}D(Lu)\mathrm{d}\Omega_1+\int_{\Omega_2}\delta(Lu)^{\mathrm{T}}D(Lu)\mathrm{d}\Omega_2-\int_{\Omega_1}\delta u^{\mathrm{T}}b\mathrm{d}\Omega_1 -\int_{\Omega_2}\delta u^{\mathrm{T}}b\mathrm{d}\Omega_2-\int_{\Gamma_{t_1}}\delta u^{\mathrm{T}}\bar{t}\mathrm{d}\Gamma_{t_1}-\int_{\Gamma_{t_2}}\delta u^{\mathrm{T}}\bar{t}\mathrm{d}\Gamma_{t_2}-\int_{\Gamma_c}\delta v^{\mathrm{T}}\tau\mathrm{d}\Gamma_c- \int_{\Gamma_{u_1}}\delta\lambda^{\mathrm{T}}(u-\bar{u})\mathrm{d}\Gamma_1-\int_{\Gamma_{u_1}}\delta u^{\mathrm{T}}\lambda\mathrm{d}\Gamma_1-\int_{\Gamma_{u_2}}\delta\lambda^{\mathrm{T}}(u-\bar{u})\mathrm{d}\Gamma_2 -\int_{\Gamma_{u_2}}\delta u^{\mathrm{T}}\lambda\mathrm{d}\Gamma_2=0 \tag{24}$$

By taking a sufficiently high order of quadrature, the weak form is integrated numerically over the domain, as a function of the size of the background cells and of the nodal distribution.

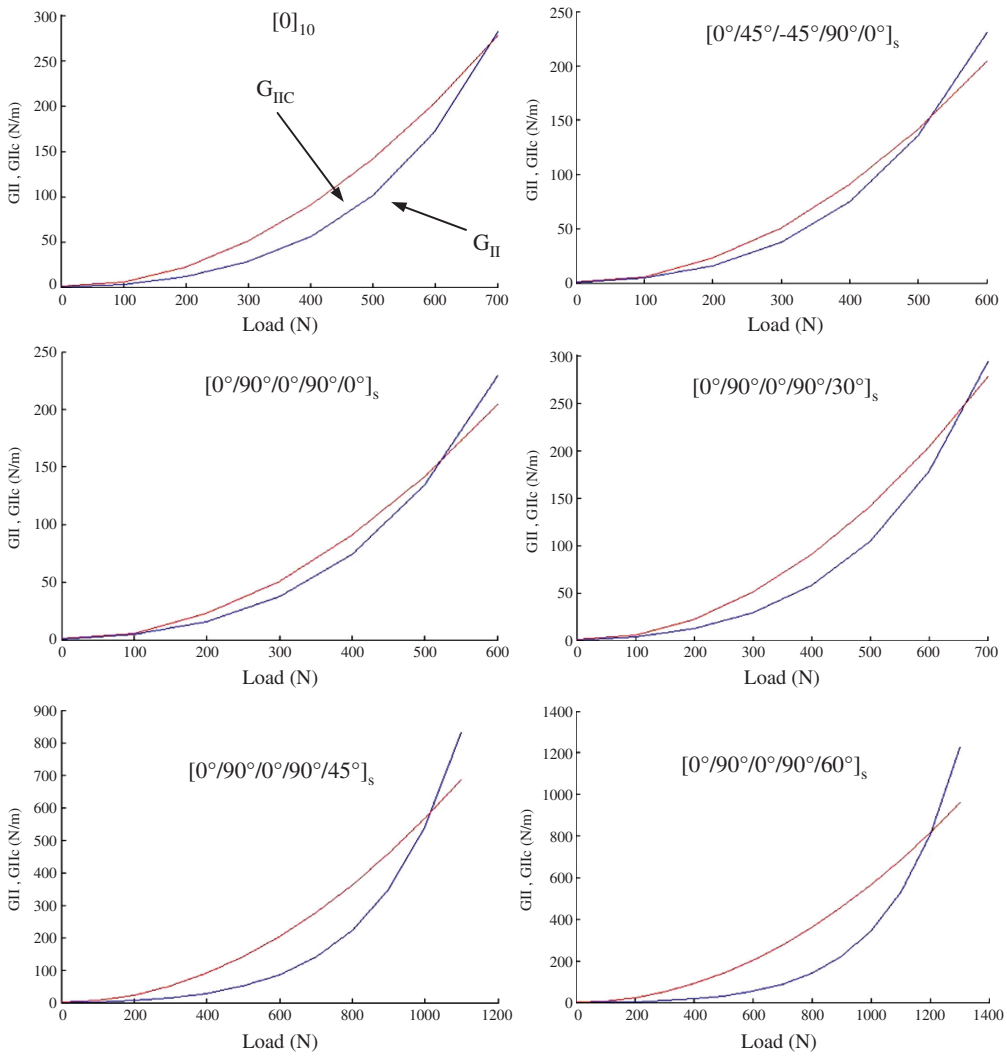

Figure 6 Energy release rate-load diagram for carbon/epoxy (AS4/3501-6) obtained from meshfree method.

$\mathbf{\Lambda}$ is a vector that collects the nodal Lagrange multipliers for all field nodes on essential boundaries:

$$\mathbf{\Lambda}=\sum_{I}^{n_i}\lambda_I^{\mathrm{T}} \tag{25}$$

If we rewrite Eq. (24), by defining **K** and **F** as the global stiffness matrix and the global force vector, respectively, we obtain

$$\begin{aligned}&\delta U_1^{\mathrm{T}}[K_1U_1+G_1\Lambda_1-F_1]+\delta\Lambda_1^{\mathrm{T}}[G_1^{\mathrm{T}}-Q_1]\\&+\delta U_2^{\mathrm{T}}[K_2U_2+G_2\Lambda_2-F_2]+\delta\Lambda_2^{\mathrm{T}}[G_2^{\mathrm{T}}-Q_2]\\&-\delta U^{\mathrm{T}}K^{\delta}U+\delta\Lambda_1^{\mathrm{T}}[G_1^{\mathrm{T}}-Q_1]+\delta\Lambda_2^{\mathrm{T}}[G_2^{\mathrm{T}}-Q_2]\\&+\delta U_1^{\mathrm{T}}G_1\Lambda_1+\delta U_1^{\mathrm{T}}G_1\Lambda_1=0\end{aligned} \tag{26}$$

where **K** is called the nodal stiffness matrix. The terms in the stiffness matrix are defined by the following equation [3]:

$$K_{IJ}=\int_{\Omega_1}B_I^{\mathrm{T}}DB_J^{\mathrm{T}}d\Omega_1+\int_{\Omega_2}B_I^{\mathrm{T}}DB_J^{\mathrm{T}}\mathrm{d}\Omega_2 \tag{27}$$

in the delaminated part:

$$\begin{aligned}K^{\delta}=\Phi^{\mathrm{T}}K(v_x,v_y)&=\begin{bmatrix}\phi_{1c}&0\\0&\phi_{1c}\\\phi_{2c}&0\\0&\phi_{2c}\end{bmatrix}\begin{bmatrix}K_x(v_x,v_y)&0\\0&K_y(v_x,v_y)\end{bmatrix}\\&=\begin{bmatrix}\phi_{1c}K_x(v_x,v_y)&0\\0&\phi_{1c}K_y(v_x,v_y)\\\phi_{2c}K_x(v_x,v_y)&0\\0&\phi_{2c}K_x(v_x,v_y)\end{bmatrix}\end{aligned} \tag{28}$$

The global force **F** is

$$\mathbf{F}=F^b+F^t, \tag{29}$$

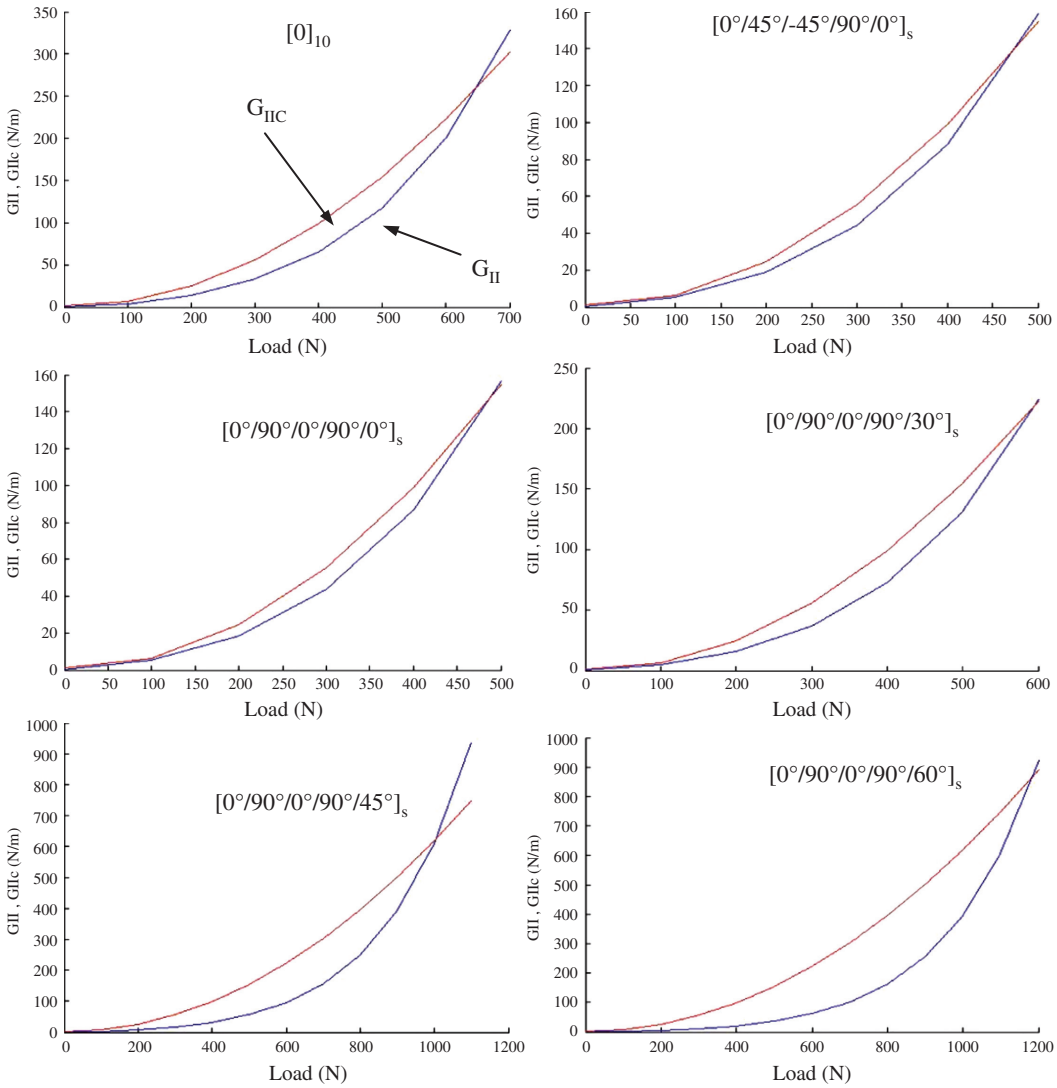

Figure 7 Energy release rate-load diagram for carbon/PEEK (AS4/APC2) obtained from meshfree method.

$$F_i^b = \int_{\Omega_1} \Phi_I^{\mathrm{T}} b \mathrm{d}\Omega_1 + \int_{\Omega_2} \Phi_I^{\mathrm{T}} b \mathrm{d}\Omega_2 \tag{30}$$

and

$$F_i^t = \int_{\Omega_1} \Phi_I^{\mathrm{T}} \bar{t} \mathrm{d}\Omega_{t_1} + \int_{\Omega_2} \Phi_I^{\mathrm{T}} \bar{t} \mathrm{d}\Omega_{t_2} . \tag{31}$$

Since both δU and $\delta\Lambda$ are arbitrary, this equation can be satisfied only if [3]

$$\begin{aligned} &K_1U_1+K_2U_2+G_1\Lambda_1+G_2\Lambda_2-F_1-F_2+K^{\delta}U=0 \\ &G_1^{\mathrm{T}}U_1+G_2^{\mathrm{T}}U_2-Q_1-Q_2=0 \end{aligned} \tag{32}$$

If it is rewritten, Eq. (32) becomes

$$\begin{bmatrix} K_1+k^{\delta} & G_1 & 0 & 0 \\ G_1^{\mathrm{T}} & 0 & 0 & 0 \\ 0 & 0 & K_2+k^{\delta} & G_2 \\ 0 & 0 & G_2^{\mathrm{T}} & 0 \end{bmatrix} \begin{Bmatrix} U_1+U \\ \Lambda_1 \\ U_2+U \\ \Lambda_2 \end{Bmatrix} = \begin{Bmatrix} F_1 \\ Q_1 \\ F_2 \\ Q_2 \end{Bmatrix} \tag{33}$$

then the solution to the whole problem can be obtained by the iterative solution of Eq. (33).

In the conventional EFGM, the stiffness matrix and load factor are computed by the Gaussian quadrature method with a background mesh.

Q and **G** are defined as a global vector form and a global matrix form, respectively:

$$Q_{IJ}^{\mathrm{T}} = -\int_{\Gamma_{u_1}} N_I^{\mathrm{T}} \bar{u} \mathrm{d}\Gamma_{u_1} - \int_{\Gamma_{u_2}} N_I^{\mathrm{T}} \bar{u} \mathrm{d}\Gamma_{u_2} \tag{34}$$

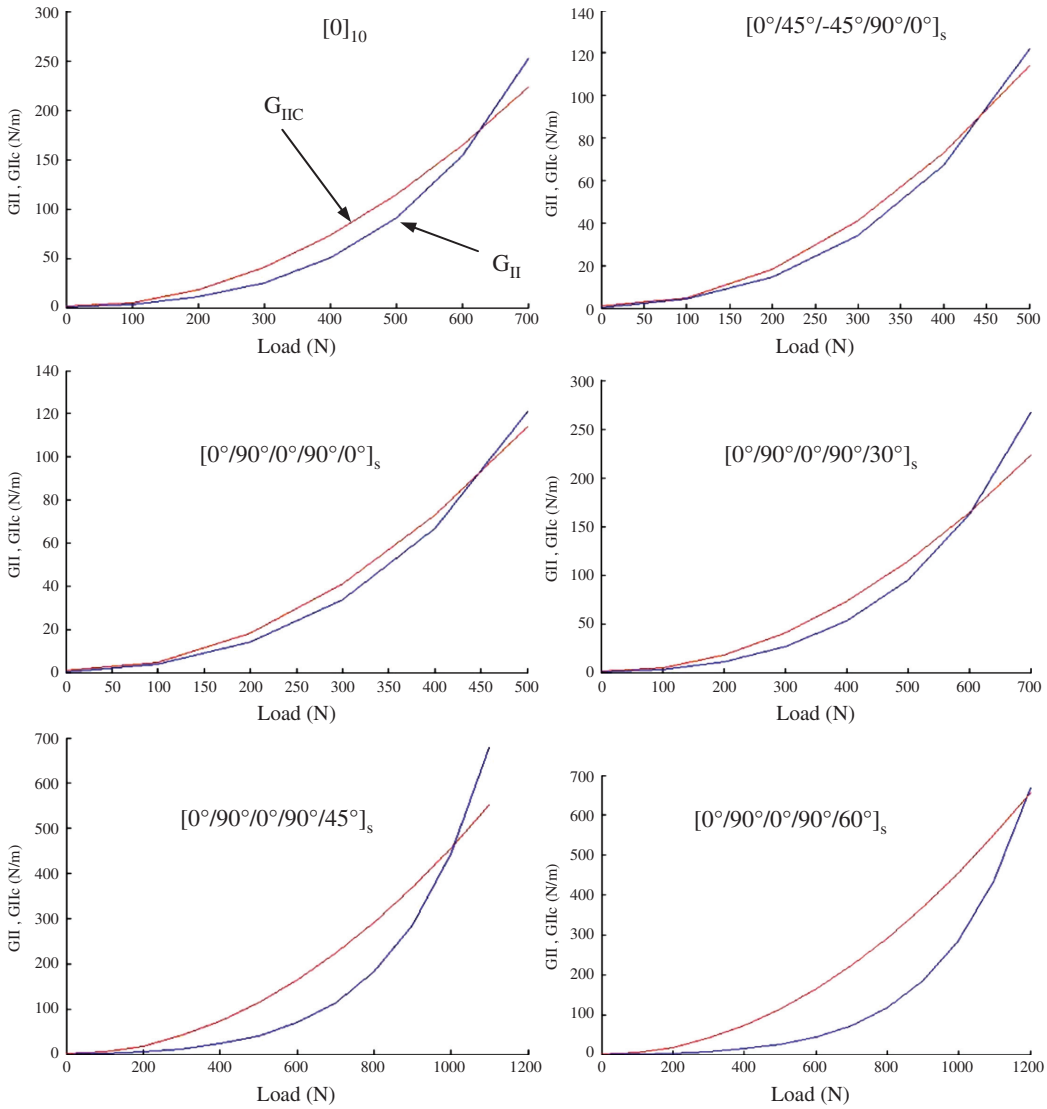

Figure 8 Energy release rate-load diagram for carbon/epoxy (IM6/SC1081) obtained from meshfree method.

$$G_{IJ}^{\mathrm{T}} = -\int_{\Gamma_{u_1}} N_I^{\mathrm{T}} \Omega_J \mathrm{d}\Gamma_{u_1} - \int_{\Gamma_{u_2}} N_I^{\mathrm{T}} \Omega_J \mathrm{d}\Gamma_{u_2} \tag{35}$$

To illustrate the applicability of the meshfree method, the delamination under mode II loading is simulated.

Table 1 Comparison of the meshfree method results of the carbon/epoxy laminate (AS4/3501-6) with $[0°]_{10}$ and $[0°/90°/0°/90°/0°]_s$.

Nodes	$[0]_{10}$		$[0/90/0/90/0]_s$	
	P (N)	*G* (N/m)	*P* (N)	*G* (N/m)
11×19	650	240.04	505	146.21
11×23	742	313.45	568	184.10

5 Numerical implementation: delamination of composite specimens

In this section, the validity and the accuracy of the meshfree EFGM are shown by determining the critical load and energy release rate in mode II delamination. To demonstrate the usefulness of the proposed method, the delamination problem is numerically analyzed by the EFG method. The fracture modes studied are mode II with an ENF test.

For the analysis of the critical load and energy release rate, some codes were developed in MATLAB. Four-point Gaussian quadrature method is employed in the EFG

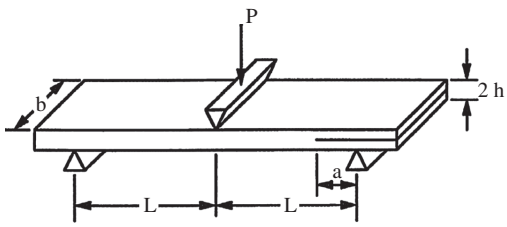

Figure 9 Specimen for end-notched flexure (ENF) specimen.

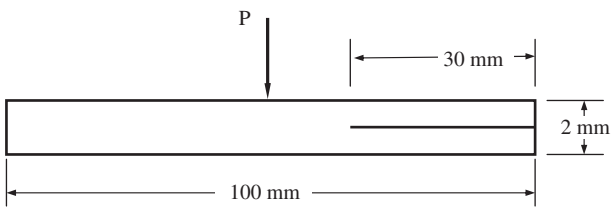

Figure 10 Specimen dimension.

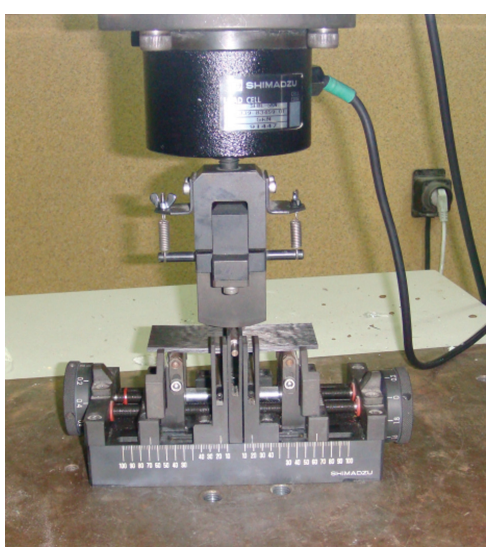

Figure 11 End-notched flexure (ENF) specimen for mode II testing mounted in the fixture.

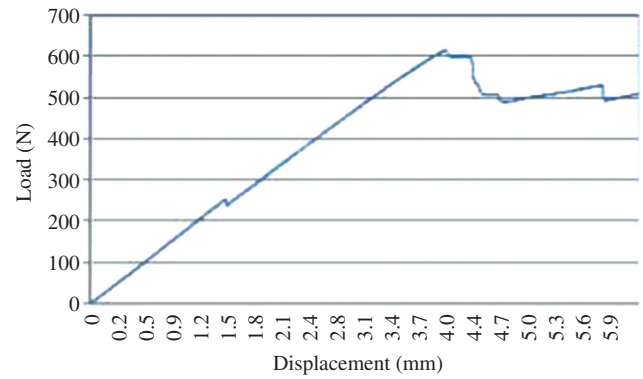

Figure 12 Load-displacement curve for $[0°]_{10}$ carbon/epoxy laminate in ENF test.

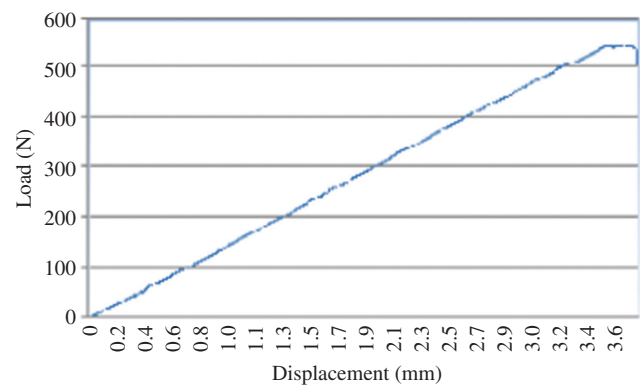

Figure 13 Load-displacement curve for $[0°/90°/0°/90°/0°]_s$ carbon/epoxy laminate in ENF test.

method. Linear basis functions in two dimensions are used. In addition, the cubic spline is taken as a weight function.

Load-energy release rate diagrams obtained from the meshfree method are shown in Figures 3–8 for different composite materials: e-glass/epoxy, s-glass/epoxy, Kevlar/epoxy (Aramid149/epoxy), carbon/epoxy (AS4/3501-6), carbon/PEEK (AS4/APC2) and carbon/epoxy (IM6/SC1081), with different orientation angles [13].

Comparison of meshfree method results of the carbon/epoxy laminate (AS4/3501-6) with $[0°]_{10}$ and $[0°/90°/0°/90°/0°]_s$ angle plies are shown in Table 1 for values of the integral for 11×19 and 11×23 background meshes.

6 Comparisons with experimental studies

To demonstrate the usefulness of the proposed method, delamination problem was investigated by analyzing the mode II delamination test. The ENF test was used to measure mode II delamination toughness. The most commonly used of these is the ENF test as it may be easily performed on thin specimens. The load measured at the onset of delamination from the precrack was used to evaluate the critical energy release rate. Tests were conducted using the ENF configuration (Figure 9), in which

Table 2 The critical load and energy release rate amount for carbon/epoxy laminate (AS4/3501-6) in mode II testing.

Orientation angle	*P* (N)	*G* (N/m)
$[0]_{10}$	614.00	278.08
$[0/90/0/90/0]_s$	547.34	220.97

Table 3 Comparison of the critical loads for carbon/epoxy laminate (AS4/3501-6) in mode II.

Orientation angle	Experimental	Meshfree method	Relative error (%)
$[0]_{10}$	614.00	650	5.86
$[0/90/0/90/0]_s$	547.34	505	7.74

Table 4 Comparison to the critical energy release rate (*G*, N/m) for carbon/epoxy laminate (AS4/3501-6) in mode II.

Orientation angle	Experimental	Meshfree method	Relative error (%)
$[0]_{10}$	278.08	313.45	12.72
$[0/90/0/90/0]_s$	220.97	184.10	16.69

a specimen with an initial mid-plane delamination at one end is loaded in a three-point bending arrangement. Although there is no universally accepted standard for mode II testing, the ENF is commonly used. End-notched flexural specimens, end-loaded split (ELS) or short-length specimens are possible test configurations to quantify delamination in mode II [22].

The ENF specimen was fabricated with carbon/epoxy (AS4/3501–6), a high-strength carbon pre-impregnated with epoxy resin-based repairing materials. The delamination cracks were simulated by Teflon films. The specimen was 100 mm long, 40 mm wide and 2 mm thick, and it had an initial crack length of 30 mm (Figure 10). Simulation of the ENF specimen was performed for two different laminate lay-ups: Type 1 $[0]_{10}$ and Type 2 $[0°/90°/0°/90°/0°]_s$.

The single-ply thickness was 0.2 mm. The mechanical properties of the unidirectional lamina are reported as follows: E_{11}=146.7 GPa, E_{22}=7.8 GPa, G_{12}=G_{13}=4.8 GPa and ν_{12}=0.29 [23].

Fracture testing was performed using universal testing machine (Shimadzu, Autograph AG-X 100 series) with a 100 kN load cell. A test sample as shown in Figure 11

Table 5 Comparison of the critical loads *P* (N) obtained from meshfree methods (nodes: 11×19).

	$[0]_{10}$	$[0/45/-45/90/0]_s$	$[0/90/0/90/0]_s$	$[0/90/0/90/30]_s$	$[0/90/0/90/45]_s$	$[0/90/0/90/60]_s$
E-Glass/epoxy	915	825	845	865	1015	1190
S-Glass/epoxy	905	810	820	875	1040	1195
Kevlar/epoxy (Aramid149/epoxy)	605	380	400	465	890	1150
Carbon/epoxy (AS4/3501-6)	650	490	505	590	965	1175
Carbon/PEEK (AS4/APC2)	620	420	455	500	930	1160
Carbon/epoxy (IM6/SC1081)	615	390	420	560	925	1170

Table 6 Comparison of the critical load *P* (N) obtained from meshfree methods (nodes: 11×23).

	$[0]_{10}$	$[0/45/-45/90/0]_s$	$[0/90/0/90/0]_s$	$[0/90/0/90/30]_s$	$[0/90/0/90/45]_s$	$[0/90/0/90/60]_s$
E-Glass/epoxy	1003	962	970	978	1073	1245
S-Glass/epoxy	995	935	955	992	1080	1287
Kevlar/epoxy (Aramid149/epoxy)	643	464	507	555	1041	1201
Carbon/epoxy (AS4/3501-6)	742	560	568	702	1062	1235
Carbon/PEEK (AS4/APC2)	702	535	540	635	1056	1210
Carbon/epoxy (IM6/SC1081)	675	508	517	638	1048	1223

Table 7 Comparison of the critical energy release rate *G* (N/m) obtained from meshfree methods (nodes: 11×19).

	$[0]_{10}$	$[0/45/-45/90/0]_s$	$[0/90/0/90/0]_s$	$[0/90/0/90/30]_s$	$[0/90/0/90/45]_s$	$[0/90/0/90/60]_s$
E-Glass/epoxy	1718.95	1399.25	1466.8	1534.34	2112.95	2902.05
S-Glass/epoxy	1523.43	1222.37	1252.99	1421.39	2012.16	2651.92
Kevlar/epoxy (Aramid149/epoxy)	344.94	138.73	153.22	205.51	746.44	1247.53
Carbon/epoxy (AS4/3501-6)	240.04	137.79	146.21	198.90	529.04	784.05
Carbon/PEEK (AS4/APC2)	239.24	110.11	128.8	156.33	536.27	833.29
Carbon/epoxy (IM6/SC1081)	173.86	70.75	81.29	143.51	391.63	625.71

Table 8 Comparison of the critical energy release rate G (N/m) obtained from meshfree methods (nodes: 11×23).

	$[0]_{10}$	$[0/45/-45/90/0]_s$	$[0/90/0/90/0]_s$	$[0/90/0/90/30]_s$	$[0/90/0/90/45]_s$	$[0/90/0/90/60]_s$
E-Glass/epoxy	2059.60	1898.96	1930.06	1961.16	2360.53	3117.57
S-Glass/epoxy	1837.58	1626.08	1696.58	1827.00	2390.62	3075.01
Kevlar/epoxy (Aramid149/epoxy)	391.43	204.80	242.54	292.23	1022.20	1357.65
Carbon/epoxy (AS4/3501-6)	313.45	179.11	184.10	279.44	640.62	865.82
Carbon/PEEK (AS4/APC2)	304.62	178.26	181.66	250.55	690.56	905.21
Carbon/epoxy (IM6/SC1081)	208.69	118.05	122.57	186.75	502.13	683.09

Table 9 Comparison of D/A_{32} (m²) and the critical loads and energy release rates for carbon/epoxy laminate (AS4/3501-6) in mode II.

Orientation angle	D/A_{32} (m²), ×10⁻¹⁰	Critical load (N) (meshfree method)	Critical energy release rate (N/m)
$[0]_{10}$	4.29	690	270.37
$[0/45/-45/90/0]_s$	2.17	520	154.17
$[0/90/0/90/30]_s$	42.3	668	254.16
$[0/90/0/90/45]_s$	87.6	1025	595.58
$[0/90/0/90/60]_s$	119	1201	817.64

was loaded with a speed of 10 mm/min. The incremental test method for mode II fracture testing which requires loading-crack propagation-unloading sequences was followed. The specimens were loaded until crack propagation occurred.

Typical load versus deflection curves (P-δ) obtained from testing the carbon/epoxy (AS4/3501-6) specimens using the ENF test are shown in Figures 12 and 13. As shown in Figure 13, when the displacement reaches about 3.4 mm, the discontinuity begins to propagate along the horizontal straight line. As the cohesive traction decreases with the increasing separation, the load-displacement curve rapidly declines as the crack propagates.

In the present study, the existing literature expression was utilized to calculate the critical strain-energy release rate for the composites [7]:

$$G_{\mathrm{IIC}}=\frac{9P^2a^2}{16E_1b^2h^3}\left[1+0.2\frac{E_1}{G_{31}}\left(\frac{h}{a}\right)^2\right] \tag{36}$$

In Eq. (36), P, a and h are defined as the applied load, the crack length and the thickness of each beam in the delaminated region, respectively. E_1 and G_{31} are the equivalent elastic flexural modulus and the equivalent transverse shear modulus of the laminate, respectively. To calculate G_{IIC} from Eq. (36), first the critical load must be determined from the experiment. The critical load and energy release rate are given in Table 2 for carbon/epoxy laminate (AS4/3501–6).

The percentage relative errors of the critical load and energy release rate are defined as follows:

$$\text{Relative error}(\%)=\frac{|E\text{-EFG}|}{E}\times 100 \tag{37}$$

where E and EFG are the critical load obtained from the experiment and the meshfree EFG method, respectively.

7 Results and discussion

In this paper, critical load and energy release rate for mode II testing of a delaminated composite for various orientation angles and materials were obtained and compared. In the experimental method, the ENF specimen was used.

Table 10 Comparison of the critical energy release rate G (N/m) obtained from meshfree methods (Nodes: 11×19).

	$[0/90/0/90/30]_s$	$[0/90/0/90/45]_s$	$[0/90/0/90/60]_s$
E-Glass/Epoxy	1534.34	2112.95	2902.05
S-Glass/Epoxy	1421.39	2012.16	2651.92
Kevlar/Epoxy (Aramid149/Epoxy)	205.51	746.44	1247.53
Carbon/Epoxy (AS4/3501-6)	198.90	529.04	784.05
Carbon/PEEK (AS4/APC2)	156.33	536.27	833.29
Carbon/Epoxy (IM6/SC1081)	143.51	391.63	625.71

Table 11 Comparison of the critical energy release rate G (N/m) obtained from meshfree methods (Nodes: 11×23).

	$[0]_{10}$	$[0/45/-45/90/0]_s$	$[0/90/0/90/0]_s$
E-Glass/Epoxy	2059.60	1898.96	1930.06
S-Glass/Epoxy	1837.58	1626.08	1696.58
Kevlar/Epoxy (Aramid149/ Epoxy)	391.43	204.80	242.54
Carbon/Epoxy (AS4/3501-6)	313.45	179.11	184.10
Carbon/PEEK (AS4/APC2)	304.62	178.26	181.66
Carbon/Epoxy (IM6/SC1081)	208.69	118.05	122.57

Table 12 Comparison of the critical energy release rate G (N/m) obtained from meshfree methods (Nodes: 11×23).

	$[0/90/0/90/30]_s$	$[0/90/0/90/45]_s$	$[0/90/0/90/60]_s$
E-Glass/Epoxy	1961.16	2360.53	3117.57
S-Glass/Epoxy	1827.00	2390.62	3075.01
Kevlar/Epoxy (Aramid149/Epoxy)	292.23	1022.20	1357.65
Carbon/Epoxy (AS4/3501-6)	279.44	640.62	865.82
Carbon/PEEK (AS4/APC2)	250.55	690.56	905.21
Carbon/Epoxy (IM6/SC1081)	186.75	502.13	683.09

The obtained results from experimental method were supported by the meshfree and finite element numerical methods. A comparison of the critical loads and energy release rate is given in Tables 3 and 4.

In Tables 3 and 4, the relative error percentages of the experimental data and the meshfree EFG are evaluated using both $[0]_{10}$ and $[0/90/0/90/0]_s$ lay-up. The relative error percentages of the critical load and energy release rate are 5.86 and 12.72 for carbon/epoxy (AS4/3501-6) with the $[0]_{10}$ lay-up. Similarly, it is seen that the relative error percentages of the critical load and energy release rate are 7.74 and 16.69 with the $[0/90/0/90/0]_s$ lay-up. The meshfree EFG results for the $[0]_{10}$ lay-up show good convergence and agreement with experimental data. The meshfree EFG method for the $[0]_{10}$ lay-up is computationally more effective than that for the $[0/90/0/90/0]_s$ lay-up.

In addition to study the effects of background meshes, the critical load and the energy release rate for two different background meshes with equivalent interval sizes were calculated in the meshfree EFGM. The critical load and the energy release rate are presented using angle-ply $[0]_{10}$, $[0/45/-45/90/0]_s$, $[0/90/0/90/0]_s$, $[0/90/0/90/30]_s$, $[0/90/0/90/45]_s$ and $[0/90/0/90/60]_s$ laminates with mid-plane delamination with six different composite materials. A comparison of the critical loads and the energy release rate for values of the integral for 11×19 and 11×23 background meshes is given in Tables 5–12.

As can be easily observed, the maximum critical load was obtained for e-glass/epoxy with the $[0/90/0/90/60]_s$ angle ply for 11×19 and 11×23 background meshes. The critical buckling loads with 11×19 and 11×23 background meshes were 1190 and 1215 N, respectively, for the $[0/90/0/90/60]_s$ angle ply. A similar study of mesh size effect was repeated for the critical energy release rate. The critical energy release rate calculated using a mesh size of 11×19 and 11×23 was 2902.05 and 3117.57 N/m, respectively, for e-glass/epoxy with the $[0/90/0/90/60]_s$ angle ply. Tables 5–8 show that the maximum critical load and the energy release rate predicted by the meshfree EFGM converge when increasing the background meshes.

As shown in Table 9, it is seen that D/A_{32} affects the critical load and energy release rate values directly. The maximum and the minimum critical loads and energy

Table 13 Comparison of D/A_{32} (m^2) and the critical loads, energy release rates for carbon/epoxy laminate (AS4/3501-6) in Mode-II.

Orientation angle	D/A_{32} (m^2) $\times 10^{-10}$	Critical Load (N) (meshfree method)	Critical energy release rate (N/m)
$[0]_{10}$	4.29	690	270.37
$[0/45/-45/90/0]_s$	2.17	520	154.17
$[0/90/0/90/30]_s$	42.3	668	254.16
$[0/90/0/90/45]_s$	87.6	1025	595.58
$[0/90/0/90/60]_s$	119	1201	817.64

release rates were obtained for the $[0/90/0/90/60]_s$ and $[0/45/-45/90/0]_s$ orientation angles, respectively.

8 Conclusions

In this paper, both numerical and experimental investigations are presented for the delamination under mode II loading, detailing the derivation of the formulations in numerical simulations of fracture. Based on the results of this study, the following conclusions can be drawn:

- It has been shown that the mode II delamination behavior of fiber-reinforced laminated composite beams could be analyzed by using a meshfree EFG method. Even though the node distribution used in this study was selected as uniform, node scattering could be changed to take into account high stress variation around the crack tip. This will help to improve the accuracy of the analysis.
- The experimental results and closed form solution were used together to calculate the mode II energy release rate for only one composite material having two different lay-ups. The critical load and energy release rate results of meshfree EFG and the FEM were compared with each other as a verification of the EFGM. Results obtained from the meshfree method showed very good agreement with experimental evidences for single-mode delamination under mode II loading. Therefore, the meshfree method is capable of accurately predicting delamination onset.
- In the meshfree method, critical loads and energy release rates are increased by an increase in the number of nodes. That is because the node density in the analysis increased everywhere including in the crack tip region. A relatively fine background mesh helps the analysis to estimate the critical load and energy release rate more accurately. Although the uniform mesh density was used in the analysis, for better performance varying the node density can be used such that more nodes may be placed around the crack tip while fewer nodes are used in the other regions.
- The maximum and the minimum critical loads and energy release rates were obtained for the $[0/90/0/90/60]_s$ and $[0/45/-45/90/0]_s$ orientation angles, respectively (Table 13). Since mode II energy release rate was calculated by using Eq. (17), where out-of-plane stress is given by

$$\tau_{\gamma} = DA_{32}^{-1} N_y \tag{38}$$

- the value of the expression D/A_{32} affects the critical load and energy release rate values directly.
- Results obtained from the meshfree method showed very good agreement with experimental data for single-mode delamination under mode II loading. The results presented will help in the implementation of numerical analysis techniques that protect numerical accuracy while minimizing computational expense. Consequently, the meshfree method could be used effectively to study delamination growth in composite laminates and it is especially suitable for the simulation of complex delamination patterns that are difficult to model using other numerical methods.

Received May 6, 2013; accepted July 6, 2013; previously published online August 8, 2013

References

[1] Alfano G, Criseld MA. *Int. Num. Met. Eng*. 2001, 50, 1701–1736.
[2] Allix O, Daudeville L, Ladevèze P. *Compos. Eng*. 1995, 5, 17–24.
[3] Barbieri E, Meo M. *Comput. Sci. Tech*. 2009, 69, 2169–2177.
[4] Belytschko T, Gu L, Lu YY. *Model Sim. Mat. Sci. Eng*. 1994, 2, 519–534.
[5] Belytschko T, Dolbow J. *Arch. Comput. Meth. Eng*. 1998, 5, 207–241.
[6] Beghini M, Bertini L, Forte P. *Comput. Sci. Tech*. 2006, 66, 240–247.
[7] Berry JP. *J. Appl. Phys*. 1963, 34, 62–68.
[8] Borst R, Remmers JJC. *Comput. Sci. Tech*. 2006, 66, 713–722.
[9] Camanho PP, Davila CG, De Moura MF. *J Compos Mat*. 2003, 37, 1415–1424.
[10] Curiel SJL, Karapurath N. *Comput. Sci. Tech*. 2012, 72, 788–791.
[11] Guiamatsia I, Falzon BG, Davies GAO. *Key Eng. Mat*. 2008, 383, 53–66.
[12] Guiamatsia I, Falzon BG, Davies GAO, Iannucci L. *Comput. Sci. Tech*. 2009, 69, 2640–2648.
[13] Hesar GG. Kompozit Malzemelerde Delaminasyon Davranışının Ağsız Yöntemler ile Analizi (In Turkish). M.Sc. Thesis, Ege University Izmir, Turkey, 2012.
[14] Liew KM, Zhao X, Ferreira AJM. *Comput. Struct*. 2011, 93, 2031–2041.
[15] Most T, Bucher C. *Eng. Anal. Bound. Elem*. 2008, 32, 461–470.
[16] Pekedis M. Ağsız Yöntemlerle Yapısal Analiz (In Turkish). M.Sc. Thesis, Ege University Izmir, Turkey, 2008.
[17] Pantano A, Averill RC. *Int. J. Sol. Str*. 2004, 41, 3809–3831.
[18] Samborsky DD, Wilson TJ, Agastra P, Mandell JF. *J. Sol. Ener. Eng*. 2008, 130, 1–22.

[19] Sun Y, Hu YG, Liew, KM. *Int. J. Eng. Sci.* 2007, 45, 541–553.
[20] Turon A, Camanho PP, Costa J, Davila CG. *Mech. Mat.* 2006, 38, 1072–1089.
[21] Turon A, Davila CG, Camanho PP, Costa J. *Eng. Frac. Mech.* 2007, 74, 1665–1682.
[22] Verdiere MC, Skordos AA, Walton AC, May M. *Eng. Frac. Mec.* 2012, 96, 1–10.
[23] Yılmaz B. Karbon Fiber Kompozit Ayak Protezi Tasarım ve İmalatı (In Turkish). M.Sc. Thesis, Ege University Izmir, Turkey, 2009.